Detector upgrade in EMIR@GTC: on-sky performances

Francisco Garzón[*1,2], Sergio Fernández-Acosta[3], Peter Hammersley[4], Enrique Joven[1,2], Anthony Russo[3], Josefina Rosich[1,2]
[1]Instituto de Astrofísica de Canarias, La Laguna, Spain; [2]Departamento de Astrofísica, Universidad de La Laguna, Spain; [3]GRANTECAN S.A., La Palma, Spain; [4]European Southern Observatory, Garching bei München, Germany

ABSTRACT

EMIR was shipped to the GTC on May 2016 and had its first light on June 2016. Since the beginning, the EMIR performances have been severely hampered by the many instabilities in the infrared detector, a 2048x2048 Hawaii2, built with the old original technology of the Teledyne Hawaii series. Despite of this, the instrument has proven to be powerful enough so as to produce a significant number of important scientific contributions. Starting in 2020, we initiated a new project aimed at equip EMIR with a most modern detector array, free from the artifacts that contaminated the observations with the old one. As a results EMIR has recently been upgraded with a new Hawaii2RG infrared detector which has superior performances virtually in every aspect compared with the old one. Not only the new detector is more sensitive, virtually in every aspect, compare with the old one but it also lacks the many instabilities of the original detected that have severely hampered the performances of EMIR, while it is not free from artifacts that increases the noise in the measurements. This is particularly noticeable under high illumination conditions, i.e. broad brand imaging, as it will be shown below. In addition, the new detector sits on a remotely operated gimbal mount that permits an exquisite alignment in the field of view. The detector is controlled by the SIDECAR integrated controller and a Markury Scientific MACIE interface card over IP communication.

Keywords: detectors, near infrared, multi-object spectrographs

1. INTRODUCTION

EMIR[1] is a near-infrared multi-object spectrograph operating in the range of 1 to 2.5 μm, which form part of the suite of common user instruments in the GTC. EMIR (*Espectrógrafo Multiobjeto InfraRrojo*, Multi-object Infrared Spectrograph) has been developed mainly at the IAC, with the participation of the UCM (Madrid) and the French institutes Observatoire de Toulose and Observatoire de Marseille. Wide-field image and multi-object and long-slit spectroscopy observation modes are available, with spectral resolutions between 1000 and 5000. For more details, refer to the instrument web sites at the IAC and GRANTECAN, http://research.iac.es/proyecto/emir and http://www.gtc.iac.es/instruments/emir/emir.php. Its first light took place in mid-2016, although the commissioning of the different observation modes lasted until well into 2018, given the high complexity of the systems that equip the instrument. As of that date, we began an intense scientific verification campaign that revealed, in addition to the capabilities of the instrument, the need to replace the detector, which is too noisy and unstable, with another of the latest generation.

To this end, we started in 2021, right after the pandemic, the tasks aimed at equipping the instrument with a most modern detector array, a Hawaii2RG. Together with the replacement of the detector itself, we also added the substitution of the Gimbal mount's angle adjustment micrometre screws with new piezoelectric actuators that can be remotely operated once the system had been cooled down. This last task resulted in the complete redesign and building of a new detector mount on which the actuators can be integrated. The new detector was received by the end of 2022 and accepted at the IAC after a test campaign on which the top-level requirements were verified.

By May 2023, EMIR was sent off its location at the Nasmyth platform of the GTC to the clean room within the premises of the telescope at the summit. Then, the instrument was disassembly to a level on which the Detector Translation Unit (DTU) housing the detector mounting could be dismounted. The new detector unit, sited in the motorized Gimbal mount, was then attached to the DTU, aligned and integrated back into its position at the instrument optical bench. Several quick

* francisco.garzon@iac.es

Ground-based and Airborne Instrumentation for Astronomy X, edited by Julia J. Bryant, Kentaro Motohara, Joël R. D. Vernet, Proc. of SPIE Vol. 13096, 1309627
© 2024 SPIE · 0277-786X · doi: 10.1117/12.3017839

functional tests were run before cooling down and also after cooling, at cryogenic temperatures, to ensure the correct working of the detector and mount before warming up the instrument to proceed to install it back at the Nasmyth rotator.

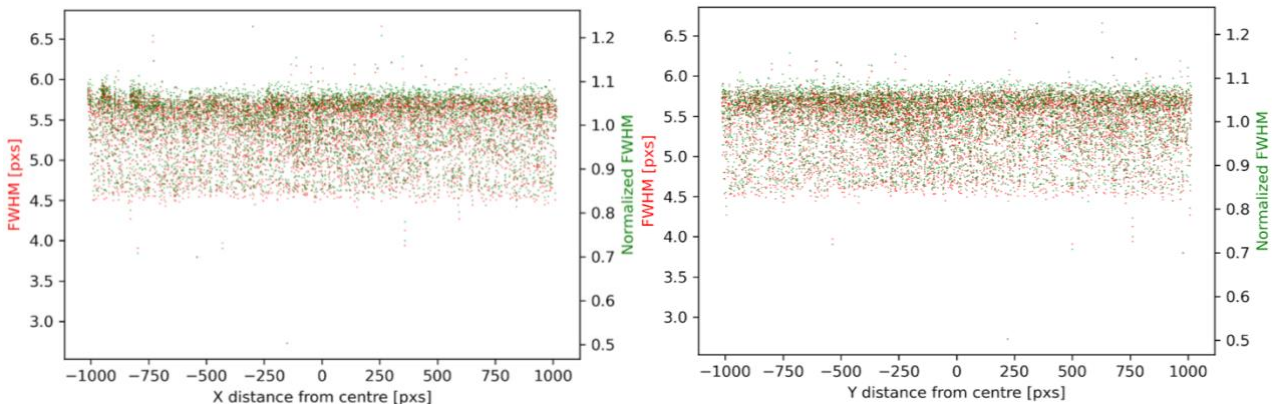

Figure 1. FWHM of point-like sources in several open clusters taken with EMIR in the J band. In red, absolute FWHM figures vs X, left panel, and Y, right panel, distances from the detector centre. In green, FWHM values are normalized to the mean of the full set.

2. FIRST RESULTS ON SKY

In August 2023, we started observing in a series of technical nights dedicated to asses and measure the real performance of the new detector and of the instrument in general. At first, we proceeded aligning the tilt angles of the mount with respect to the instrument focal surface. In Figure 1, we show the how, after the alignment process, the detector surface alignment is extremely parallel to the instrument focal surface, as the image size shows a high uniformity across the full field of view.

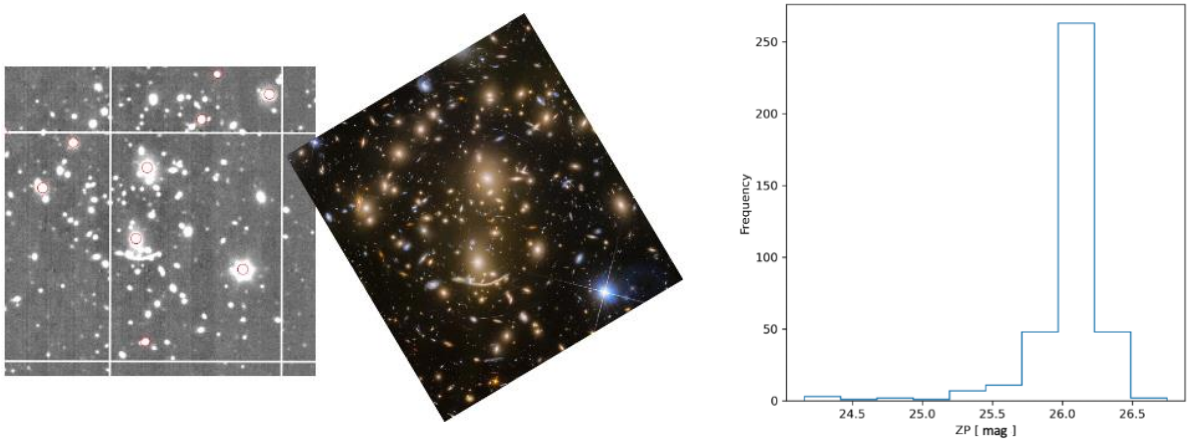

Figure 2. Left: Central region of the cluster of galaxies Abell 370. The EMIR J image, on the left, has been produced combining 400 CDS images, 10s each; on the right, a HST Frontier Field multicolor image of the same cluster, for comparison purposes. Red circles on the EMIR image are the positions of the GAIA DR3 sources found on the field. Right: histogram of zero points (ZP) in the J band derived from a series of images of open clusters. There is a shift of about half a magnitude in the ZPs.

Together with an excellent alignment, the detector also shows a remarkable good photometric uniformity and sensitivity. Figure 2 depicts a deep image taken with EMIR in the J band of Abell 370, with very little data treatment, that can be compared with the same field in a multicolor image from the HST. The photometric uniformity can be seen in the left panel of Figure 2, where a histogram of the J band zero point derived from open cluster images taken with EMIR and cross-correlated with 2MASS are shown. The sources are distributed all over the frame and is of note the high concentration of values around the mean. Finally, Table 1 shows the measured ZP in the JHKs bands compared with the same figures with the old detector. To transform from counts to electrons, we have used the gain measured in laboratory test of 3.3 e^- /adu, while this value is yet a bit uncertain as we have obtained slightly different ones in different measurements, using

several data treatment schemes. It has to be mentioned that there still artifacts in the detector readout scheme, that will be referred to in the next section, that have some influence in the photometry. We are currently working on eliminating these effects that would result in even better improvement of the sensitivity. For the time being, and as will be shown below, the way we are alleviating these instabilities consists mainly in reducing the detector duty cycle. We have not yet repeated these photometric observations with this method implemented.

Table 1. Zero points measured in the 3 NIR bands JHKs. In parentheses, the magnitudes with the old detector

Band	mag @1adu/s	mag @1e$^-$/s
J	25.570 ± 0.179 (25.14)	26,848
H	25.746 ± 0.101 (25.26)	26,942
Ks	25.203 ± 0.176 (24.81)	26,476

We have also taken a series of measurement of dark current at the detector, consisting in long integration times with the instrument fully closed (entrance window, Cold Slit Unit, grism wheel, filter wheel). Results are given in Figure 3, that show that there is no real impact of the working temperature of the detector in this range between 40K and 60K. Due to better behaviour with respect to persistence, we are operating the detector at 40K. In the same set of measurements, we have obtained a figure for a readout noise in single read of 20.12 e$^-$ as a mean value over the 32 outputs of the array.

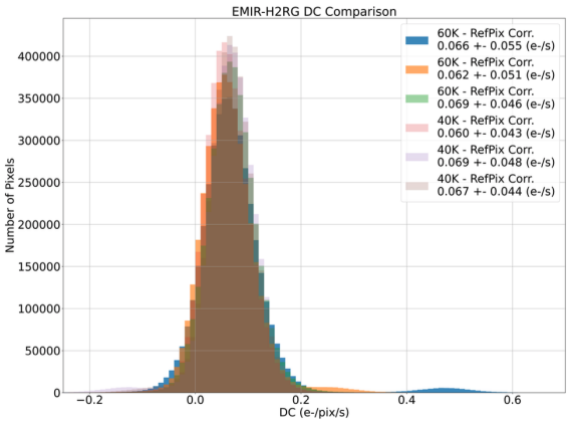

Figure 3. Histograms of dark current measurements at two temperatures. No real differences are observed between them.

3. DETECTOR INSTABILITIES MEASURED SO FAR

3.1 Non linearity

Non-linear effects in the conversion from charge to voltage, and then to counts, in the near infrared detectors are well known since long ago (see for example [2] and [3]), and several methods to correct them can be found in the literature. In Figure 4, we show how this effect is present in the EMIR H2RG and one potential method to account for it. In Figure 4, blue diamonds represent the raw data, red squares are the fit to the ramp following the prescription in [4] and the green symbols depict the linear part of the previous fits. Left panel of Figure 4 shows a ramp taken under low illumination, which shows very little difference between the green and the blue, while the right panel, that plots a heavily illuminated ramp, exhibit marked difference between both. That shows that, as expected, non linear effects are more acute under high illumination.

It is important for a multipurpose instrument like EMIR to correct this effect, as the broad band image mode can collect several thousand counts per second just from the thermal emission of the atmosphere, the redder the band the higher the counts. So, in CDS readout mode (Fowler sampling with one read per group), which is the EMIR standard for image mode, the cost of non correcting the lack of linearity in the measurement will result in a loss of signal.

The plan to deal with this effect, following [4], is to derive a non-linearity correction using well defined ramps, in URG read mode, that can be applied when only two read frames are available, as the in the CDS read mode. We are working with several schemes to apply this correction. At this time, the best results are obtained deriving a ratio of non linearity (RNL) per average detector column, by averaging some set of measurements that can cover a wide range on input fluxes.

Low fluxes are excluded from the average since they do not show significant non linearities. The fitted RNLs are then removed from the raw data and a second fit is performed on the residuals. In Figure 5 we show the type of correction proposed for one of the 32 detector outputs. The blue, green and magenta dots show the statistics of the RNL that are derived using the 64 columns of the given detector output. These values are read in the left Y axis of Figure 5. The red points in Figure 5, together with their error bars, gives an idea of the quality of the linear signal recovery. They show the difference in percentage, in right Y axis, between the signal obtained fitting the raw ramp after the double RNL correction and the linear fit of the ramp following [4], i.e. green points in Figure 4.

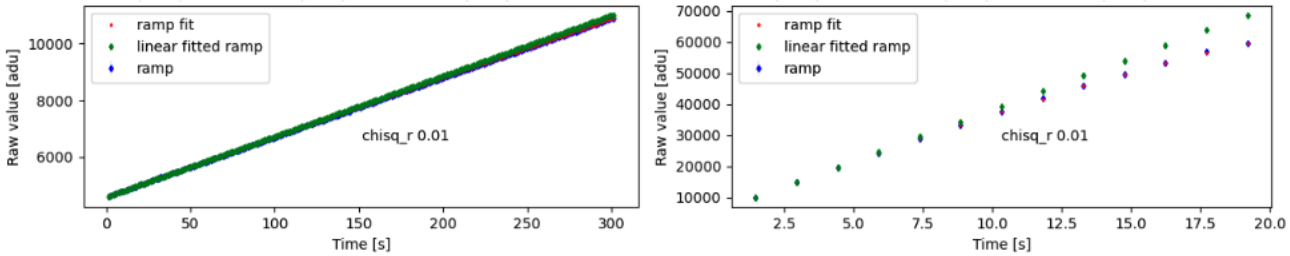

Figure 4. Ramps taken at different illuminations, with increasing flux left to right.

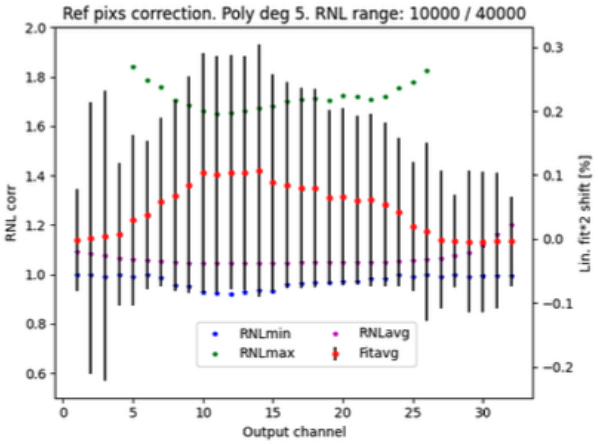

Figure 5. Non linearity ratio (RNL) in a set of measurements like in figure 4, left Y axis, together with the average deviation on linearity after applying a polynomial double fit to the data, right Y axis. See text for details.

3.2 Drift in signal after reset

The most harmful effect in the detector signal that we have observed so far is an offset seen in the raw counts in both read modes, URG & FS, when taking a series of ramps in a sequence. The offset in slope can be as high as few kadu/s, depending on incoming flux, between the first ramp and the rest of the sequence. The offset is more noticeable in the raw counts of the frame taken immediately after the last reset, but translate also to the final slope, while at smaller level. We have performed many tests, that are still ongoing, that demonstrate that the offset has more to do with the illuminating flux and less with the time from the last reset. In fact, using the smallest portion of the detector frame that permits the current detector controller, so as the readout time is very short compared with the full detector frame time, we have verified that this effect is still present. So, it seems not to depend on the time between last reset and first read, which is rather short in this case.

In Figure 6 we show this effect in a series of measurements. We cover the full list of reset types available, that are given in the text at the bottom. Per reset type, we take 3 sequences of 5 ramps each, separated 3 minutes in time, and with a number of resets after each ramp on the sequence varying from 1 to 3. Each point in Figure 6 is derived by averaging a central section of 200x2040 pxs on each frame. Big red asterisks in Figure 6 show the initial signal of each ramp obtained by a linear fit on the full frame sequence. It is remarkable the difference between the first ramp and the rest of the sequence in the 1 reset series. This difference become smaller as the number of resets increases and virtually disappear with 3 resets per ramp. The red number on top of each sequence represents a sort of signal to noise ratio, as it is the mean value divided by the standard deviation of the signals. Big green asterisks in Figure 6 show the same magnitudes previously described,

but after removing the initial jump on each ramp. In this case, the drift effect decreases but are still present. Moreover, the signal fluctuates heavily depending on the input flux, effect that cannot be seen in Figure 6, and the results are not reliable.

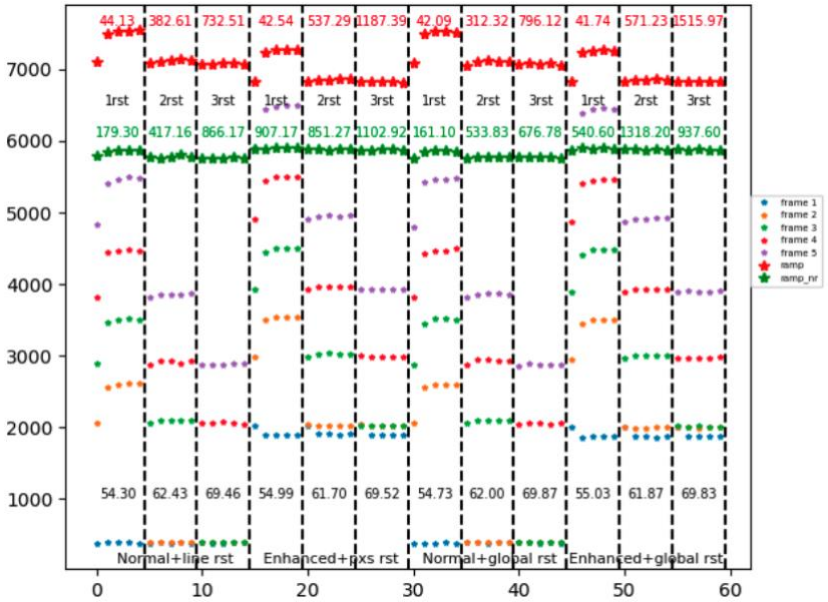

Figure 6. Sequences of 5 ramps, 5 reads each, covering all the reset types, described in the text at the bottom, and with 1 to 3 resets before reading the next ramp in the sequence. Y axis show the raw counts in adu. See text for details.

At present, and as can be inferred from Figure 6, we can only fix this effect adding more resets, which translates in a poor duty cycle in CDS modes, as each reset takes one full frame time, which is a bit below 1.5s. Other readout schemes permit faster resets, see [5] and [6], but the existing firmware in our controller do not contemplate this option. We are currently evaluating ways of implementing fast reset within the existing control infrastructure, but other alternatives are also under consideration.

4. CONCLUSIONS

The installation of the new Hawaii2RG infrared detector has greatly improved the performances of EMIR. There are still undesirable effects that do not preclude the use of the instrument. We are working hard in devising ways to overcome these artifacts that would result in ever greater gain in instrument performances.

REFERENCES

[1] Garzón, F. et al.," EMIR, the near-infrared camera and multi-object spectrograph for the GTC", 2022, A&A, 667.

[2] Plazas, A. A. et al., "Nonlinearity and pixel shifting effects in HXRG infrared detectors", https://arxiv.org/pdf/1703.08205.

[3] Robberto, M., "Implementation of a new algorithm for the correction of non-linearity in JWST detectors", JWST-STScI-002346.

[4] Canipe, A. et al., "A New Non-Linearity Correction Method for NIRCam", JWST-STScI-005167, SM-12

[5] Storz, C. et al., "Standard modes of MPIA's current H2/H2RG-readout systems", Proc. SPIE Vol. 8453, 84532E

[6] Smith, R., "H2RG readout for efficient coadds of bright image", https://nexsci.caltech.edu/committees/JWST/smith_bright_objects.pdf